

Bandwidth-induced saturation in multimode fiber-based absorbers

Kfir Sulimany, Dotan Halevi, Omri Gat, and Yaron Bromberg

Racah Institute of Physics, The Hebrew University of Jerusalem, Jerusalem 91904, Israel

Abstract

Multimode fiber-based saturable absorbers enable mode-locking in lasers, generating ultrafast pulses and providing an exceptional platform for investigating nonlinear phenomena. Previous analyses in the continuous wave (CW) limit showed that saturable absorption can be obtained due to nonlinear interactions between transverse modes. We find experimentally that saturable absorption can be achieved thanks to the interplay of single-mode fiber nonlinearity and the wavelength-dependent linear transmission of the multimode fiber, even with negligible intermodal nonlinearities. We further show that even when intermodal nonlinearities are significant, the CW analysis may not be sufficient for long multimode fibers. Understanding the underlying mechanisms of multimode fiber-based saturable absorbers opens new possibilities for developing programmable devices for ultrafast control.

A saturable absorber is an optical device with a transmission that depends on the intensity of the incident light, selectively absorbing low-intensity light while allowing transmission of sufficiently high intensities. These devices are extensively used for ultrafast pulse generation in passively mode-locked lasers [1, 2]. When integrated into a laser cavity, high-power pulses stimulated by random fluctuations in the intra-cavity field can be preferentially transmitted by the saturable absorber, while the low-power wings of the pulses are blocked. Over multiple round trips, this process leads to mode-locking.

Traditionally, saturable absorbers are implemented in mode-locked fiber lasers by utilizing semiconductor saturable absorber mirrors [3], as well as carbon nanotubes [4] and two-dimensional nanomaterials [5–7]. These methods, however, still possess certain limitations such as low damage thresholds, narrow operational bandwidths, and complex manufacturing processes. Another class of effective saturable absorbers is based on optical nonlinearities, such as nonlinear polarization rotation [8], and nonlinear loop mirrors [9, 10]. The former method exhibits low environmental stability and its self-starting behavior is challenging, and the latter entails a complex cavity structure. Consequently, a growing research interest is exploring new mechanisms to achieve mode-locking in fiber lasers.

A multimode nonlinear interference-based saturable absorber was theoretically proposed a decade ago by Nazemosadat and Mafi [11]. This device consists of a sandwiched graded-index (GRIN) multimode fiber spliced at both ends to two single-mode fibers. The device has clear advantages, including low saturation powers, large modulation depths, ultrafast response time, easy fabrication, wide response band, and high damage thresholds [12, 13]. Therefore, in the last decade, dozens of nonlinear interference-based saturable absorbers im-

plemented in ultrafast mode-locked lasers operating at $1.55\mu\text{m}$ [14–39], in $1\mu\text{m}$ [40–55], and in $2\mu\text{m}$ [56–60].

So far, the analysis of multimode fiber-based saturable absorbers has been limited to the continuous wave (CW) limit, where the combination of linear self-imaging in GRIN multimode fibers and nonlinear self-focusing due to the Kerr effect leads to a power-dependent transmission [11, 61, 62]. This mechanism can drive mode-locking in fiber lasers, yet it neglects spectral effects in multimode fibers and predicts weak saturations for typical peak powers in mode-locked lasers.

In this work, we study experimentally a multimode fiber-based saturable absorber and analyze its nonlinear features numerically. We find that the interplay between the linear wavelength-dependent transmission of the multimode fiber and the nonlinear spectral broadening in the first single-mode fiber leads to saturable absorption for typical peak powers in mode-locked fiber lasers. Lastly, we study numerically the effect of the nonlinearity in the multimode fiber in our saturable absorber, obtaining insight that paves the way for developing programmable saturable absorbers for ultrafast dynamics by all-fiber spectral modulation techniques [63].

To study the transmission properties of the saturable absorber, we sandwiched a 2 m -long section of GRIN multimode fiber (OM1 62.5/125 μm , Corning) between two 1 m-long sections of single-mode fiber (SMF, Thorlabs HP780), as illustrated in Fig. 1. We inject short pulses from a Ti:Sapphire laser (Coherent Chameleon Ultra II, 680–1060 nm, 140 fs duration, 80 MHz repetition rate) into the device. We illustrate the power spectrum of the pulse in Fig. 1. In the first SMF, the input pulse experiences spectral broadening due to self-phase modulation. When the pulse is coupled into the GRIN MMF, a few transverse modes are excited. The coupling to the second SMF now depends on the wavelength-dependent

interference between the transverse modes at the output of the GRIN fiber. The transmission through the device thus depends on the spectral broadening in the first SMF and is therefore power-dependent.

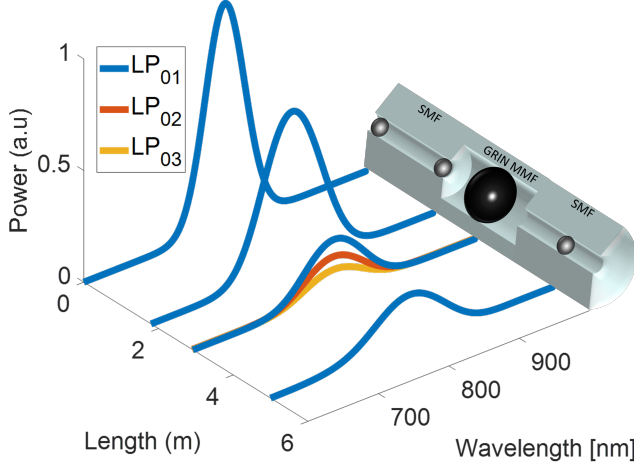


Figure 1: **Illustration of pulse propagation in a multimode fiber-based saturable absorber.** An input Gaussian pulse is coupled to a saturable absorber consisting of a graded-index (GRIN) multimode fiber sandwiched between two single-mode fibers (SMF). Self-phase modulation in the first SMF broadens the spectral bandwidth of the input pulse by a few nanometers. When the pulse is coupled to the GRIN multimode fiber, it excites the first few modes of the fiber, labeled by the linearly polarized $LP_{l,m}$ modes. The device transmission, which is determined by the wavelength-dependent coupling to the second SMF, depends on the spectral broadening in the first SMF and is therefore power-dependent.

Fig. 2(a) presents the measured power transmitted through the saturable absorber, normalized by input power, as a function of the central wavelength of the pulse λ_0 and its peak power. At low peak powers, fringes appear in the spectrum due to the phase velocity difference between the modes in the MMF, with a few nanometers scale of change. These fringes disappear above peak powers of ~ 2 kW, where spectral broadening in the first SMF becomes comparable with the MMF spectral scale of change. The pulse temporal broadening in the SMF, measured by an optical spectrum analyzer (Yokogawa AQ6374), is presented in the supplementary information, section 1. The fading of the fringes leads to saturated absorption in wavelengths that exhibit destructive interference in the linear regime, for example in 795 nm marked by the white dashed line. To highlight the saturated absorption, we present in Fig. 2(c) a cross-section of Fig. 2(a) at $\lambda_0 = 795$ nm. The saturation power, of less than 1 kW, is a few orders of magnitude lower than that obtained in the continuous wave limit [11].

To investigate the absorption mechanisms of the SMF-MMF-SMF configuration, we numerically solved the

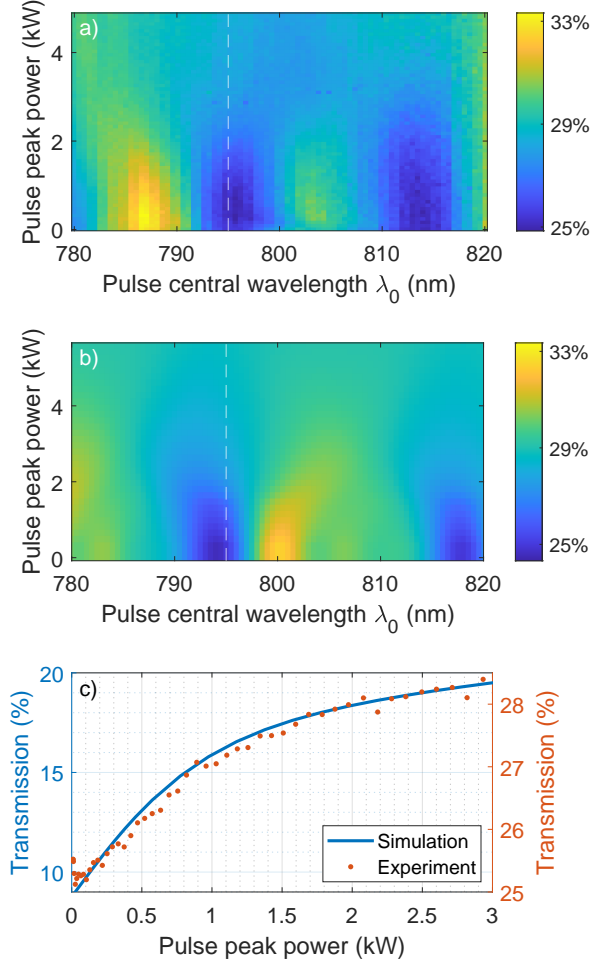


Figure 2: **Wavelength-dependent transmission of a multimode fiber-based saturable absorber.** (a) Transmission measurements and (b) simulations as a function of the central wavelength of the pulse λ_0 and its peak power. At low peak powers, spectral fringes appear due to the phase velocity difference between the modes. These fringes disappear gradually above peak powers of ~ 2 kW when the pulse spectrum starts to broaden due to self-phase modulation. Saturated absorption is obtained for central wavelengths that exhibit destructive interference in the linear regime, for example, $\lambda_0 = 795$ nm, marked by the white dashed lines and plotted in (c).

multimode nonlinear Schrödinger equation (MM-NLSE) using the numerical solver developed by Wright et al. [64]. The MM-NLSE is given by:

$$\frac{\partial A_k}{\partial z} = i \sum_n \frac{\beta_n^{(k)}}{n!} \left(i \frac{\partial}{\partial t}\right)^n A_k + i \frac{n_2 \omega_p}{c} \sum_{lmn} S_{klmn} A_l A_m A_n^* \quad (1)$$

where $A_k(z, t)$ is the slowly varying amplitude of mode k , z is the propagation distance along the fiber, t is time in the comoving frame, and $\beta_n^{(k)} = \partial^n \beta^{(k)} / \partial \omega^n$, $\beta^{(k)}$ being the propagation constant of mode k . The nonlinear coupling coefficients S_{klmn} are given by the overlap of the transverse waveforms of the guided modes $F_k(x, y)$:

$$S_{klmn} = \frac{\int dx dy F_k^*(x, y) F_l^*(x, y) F_m(x, y) F_n(x, y)}{\sqrt{\prod_{i=k,l,m,n} \int dx dy |F_i(x, y)|^2}} \quad (2)$$

To examine the role of nonlinear effects in the multimode fiber, we compare two sets of numerical simulations of Eq. 1. In one set we simulate the full equation and in the other, we neglect its nonlinear terms. First, we calculated the waveform of a nonlinear 200fs pulse propagating in a 1m of 4.4μm step-index SMF with an NA of 0.13. Then we calculated the overlap of the field at the output of the SMF with the guided modes of a GRIN multimode fiber with a core diameter 62.5μm. For simplifying the numerical computation we considered only the first 11 radial transverse modes of the multimode fiber, to which 97% of the energy is coupled (see supplementary information section 2 for more details). Next, we calculated the pulse waveform at the end of the multimode fiber, assuming linear propagation as explained above. Lastly, we calculated the coupling of the pulse to another 4.2μm step-index single-mode fiber.

The calculated pulse transmission as a function of pulse central wavelength and peak power is presented in Fig. 2(b), showing a qualitative agreement with the experimental results. In the experiment, the modulation depth, defined by the difference in the transmission of the high and low peak powers, is lower than in the simulation. The disagreement is due to the dependence of the modulation depth on the multimode fiber length, which was not optimized to fit the experimental results (see supplementary information, section 3). In contrast, above peak powers of 4kW the modulation depth becomes insensitive to the pulse peak power, a desired feature for saturable absorbers in mode-locked lasers. Finally, the numerical simulations that include the nonlinear terms in Eq. 1 show that in our configuration, the contribution of nonlinear effects in the multimode fiber is negligible (see supplementary information, section 3).

To expand our investigation to a regime in which intermodal nonlinearity plays an important role, we considered a case similar to the one that has been studied in the CW limit [11]. We initiated a 200fs-wide, 6.9nJ-energy Gaussian pulse, at the start of a GRIN multimode fiber. The occupation of each mode is chosen according to its overlap integral with the SMF mode profile. We considered the first 6 radial transverse modes of the multimode fiber, of which 95% of the energy is coupled. In this simulation, the pulse was transform-limited at the start of the multimode fiber, so its power was sufficient to induce nonlinearities. We calculated the nonlinear pulse prop-

agation according to Eq. (1) and then calculated the coupling transmission into a single-mode fiber.

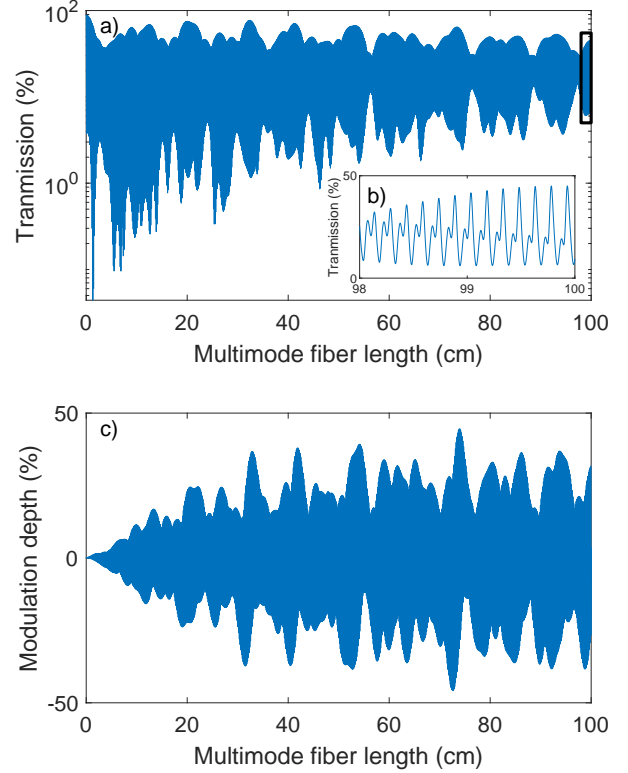


Figure 3: Saturable absorption properties as a function of multimode fiber length. The calculated coupling transmission of the graded-index (GRIN) multimode fiber to the single-mode fiber, calculated using full Eq. 1, is presented versus the multimode fiber length. As the GIMF multimode fiber length increases, the interplay between its spectral scale of change and the pulse nonlinear spectral broadening prevents the transmission from vanishing. This feature, which is desired in saturable absorbers, cannot be described in the CW limit. The transmission exhibits a fast modulation, as highlighted in the inset, showing 200μm collapse length and 1.5mm revival length. The modulation depth, panel (c) becomes significant after the first few centimeters of the fiber due to intermodal nonlinearities.

The calculated transmission from the GRIN multimode fiber to the SMF versus the GRIN multimode fiber length is presented in Fig. 3(a). As the GRIN multimode fiber length increases, the interplay between the spectral scale of change and the pulse nonlinear spectral broadening prevents the transmission from vanishing. This feature, which is desired in saturable absorbers, cannot be captured in the CW limit. The transmission shows fast oscillations, as highlighted in the inset Fig. 3(b). In this configuration, the modulation depth depicted in Fig.

3(c), is affected by both the intermodal nonlinear interference and the bandwidth of the multimode fiber. As in the experiment, the modulation depth is calculated by subtracting from the transmission obtained at high peak powers, the transmission obtained at low powers (see supplementary information section 4), and the high power pulse transmission in Fig.3(a).

Our results regarding the role of spectral effects in multimode fiber-based saturable absorbers suggest that the properties of the saturable absorber are mainly determined by the transmission at weak peak powers, which is mainly determined by linear propagation in the multimode section. It is widely recognized that interference effects in multimode fibers depend sensitively on the multimode fiber length and therefore fine-tuning is required to achieve a desired saturable absorption. Recently, we have demonstrated that the linear transmission can be controlled by applying computer-controlled mechanical perturbations [63, 65]. In the bandwidth-induced multimode fiber-based saturable absorber, therefore, fine-tuning can be achieved by all-fiber modulation. Moreover, in lasers, the optimal desired absorptive nonlinearities for self-starting and steady-state operation are often different, and thus dynamic control allows the implementation of both configurations in a single device.

Acknowledgments

The authors wish to thank F. Wise and L. Wright for making freely available the open-source parallel numerical mode solver for the coupled-mode nonlinear Schrödinger equations [64]. This research was supported by the *the ISF-NRF Singapore joint research program* (Grant No. 3538/20) and the *Israel Science Foundation (ISF)* (Grant No. 2403/20). K. Sulimany and Y. Bromberg acknowledge the support of the Israeli Council for Higher Education, and the Zuckerman STEM Leadership Program.

References

- [1] Philippe Grelu and Nail Akhmediev. “Dissipative solitons for mode-locked lasers”. In: *Nature photonics* 6.2 (2012), pp. 84–92.
- [2] Herman A Haus. “Mode-locking of lasers”. In: *IEEE Journal of Selected Topics in Quantum Electronics* 6.6 (2000), pp. 1173–1185.
- [3] Ursula Keller et al. “Semiconductor saturable absorber mirrors (SESAM’s) for femtosecond to nanosecond pulse generation in solid-state lasers”. In: *IEEE Journal of selected topics in QUANTUM ELECTRONICS* 2.3 (1996), pp. 435–453.
- [4] Sze Y Set et al. “Laser mode locking using a saturable absorber incorporating carbon nanotubes”. In: *Journal of lightwave Technology* 22.1 (2004), p. 51.
- [5] D Popa et al. “Sub 200 fs pulse generation from a graphene mode-locked fiber laser”. In: *Applied Physics Letters* 97.20 (2010).
- [6] Kfir Sulimany et al. “Bidirectional soliton rain dynamics induced by casimir-like interactions in a graphene mode-locked fiber laser”. In: *Physical review letters* 121.13 (2018), p. 133902.
- [7] Avi Klein et al. “Ultrafast rogue wave patterns in fiber lasers”. In: *Optica* 5.7 (2018), pp. 774–778.
- [8] VJ Matsas et al. “Self-starting, passively mode-locked fibre ring soliton laser exploiting non-linear polarisation rotation”. In: *Electronics Letters* 28.15 (1992), pp. 1391–1393.
- [9] NJ Doran and David Wood. “Nonlinear-optical loop mirror”. In: *Optics letters* 13.1 (1988), pp. 56–58.
- [10] Martin E Fermann et al. “Nonlinear amplifying loop mirror”. In: *Optics Letters* 15.13 (1990), pp. 752–754.
- [11] Elham Nazemosadat and Arash Mafi. “Nonlinear multimodal interference and saturable absorption using a short graded-index multimode optical fiber”. In: *JOSA B* 30.5 (2013), pp. 1357–1367.
- [12] Yaoyao Qi et al. “Recent research progress of nonlinear multimode interference mode-locking technology based on multimode fibers”. In: *Infrared Physics & Technology* 121 (2022), p. 104017.
- [13] Bo Fu et al. “Recent advances and future outlook in mode-locked lasers with multimode fibers”. In: *Applied Physics Reviews* 10.4 (2023).
- [14] Kfir Sulimany et al. “Soliton-pair dynamical transition in mode-locked lasers”. In: *Optica* 9.11 (2022), pp. 1260–1267.
- [15] Kangjun Zhao et al. “Free-running dual-comb fiber laser mode-locked by nonlinear multimode interference”. In: *Optics Letters* 44.17 (2019), pp. 4323–4326.
- [16] Liujiang Li et al. “L-band tunable and dual-wavelength mode-locked fiber laser with NCF-GIMF-based SA”. In: *IEEE Photonics Technology Letters* 31.8 (2019), pp. 647–650.
- [17] Fengyan Zhao et al. “Experimental observation of bound solitons with a nonlinear multimode interference-based saturable absorber”. In: *Laser Physics Letters* 15.11 (2018), p. 115106.
- [18] Tianyu Zhu et al. “Observation of controllable tightly and loosely bound solitons with an all-fiber saturable absorber”. In: *Photonics Research* 7.1 (2019), pp. 61–68.

- [19] Zhaokun Wang et al. "Generation of pulse-width controllable dissipative solitons and bound solitons by using an all fiber saturable absorber". In: *Optics Letters* 44.3 (2019), pp. 570–573.
- [20] Qian-Chao Wu et al. "Femtosecond soliton erbium-doped fiber laser with a symmetrical GIMF–SIMF–GIMF saturable absorber". In: *IEEE Photonics Journal* 11.6 (2019), pp. 1–9.
- [21] Yaping Gan et al. "Generation of high-order solitons with order continuously adjustable in a fiber laser based on GIMF–SIMF–GIMF saturable absorber". In: *Optics Communications* 479 (2021), p. 126441.
- [22] Jikai Chen et al. "GIMF-based SA for generation of high pulse energy ultrafast solitons in a mode-locked linear-cavity fiber laser". In: *Journal of Lightwave Technology* 38.6 (2020), pp. 1480–1485.
- [23] Jikai Chen et al. "GIMF-based SA for generation of high pulse energy ultrafast solitons in a mode-locked linear-cavity fiber laser". In: *Journal of Lightwave Technology* 38.6 (2019), pp. 1480–1485.
- [24] Guangwei Chen et al. "Generation of transition of dark into bright and harmonic pulses in a passively Er-doped fiber laser using nonlinear multimodal interference technique". In: *Infrared Physics & Technology* 112 (2021), p. 103607.
- [25] Zhaokun Wang et al. "Er-doped mode-locked fiber laser with a hybrid structure of a step-index-graded-index multimode fiber as the saturable absorber". In: *Journal of Lightwave Technology* 35.24 (2017), pp. 5280–5285.
- [26] Fengyan Zhao, Ning Li, and Hushan Wang. "Generation of a noise-like pulse from an erbium-doped fiber laser based on nonlinear multimode interference". In: *Laser Physics* 30.12 (2020), p. 125102.
- [27] Kangjun Zhao et al. "Nonlinear multimode interference-based dual-color mode-locked fiber laser". In: *Optics Letters* 45.7 (2020), pp. 1655–1658.
- [28] Hongwei Zhang et al. "C-band wavelength tunable mode-locking fiber laser based on CD-SMS structure". In: *Applied Optics* 58.21 (2019), pp. 5788–5793.
- [29] Fengyan Zhao et al. "High-energy solitons generation with a nonlinear multimode interference-based saturable absorber". In: *Laser Physics* 28.8 (2018), p. 085104.
- [30] Fengyan Zhao et al. "Ultrafast soliton and stretched-pulse switchable mode-locked fiber laser with hybrid structure of multimode fiber based saturable absorber". In: *Scientific Reports* 8.1 (2018), p. 16369.
- [31] Xin Li, DN Wang, and Jikai Chen. "Saturable absorber based on a hybrid structure of graded-index multimode fiber and graphene for a passive mode-locked erbium-doped fiber laser". In: *JOSA B* 38.7 (2021), pp. 2112–2117.
- [32] Jiaqiang Lin et al. "Wavelength switchable all-fiber mode-locked laser based on nonlinear multimode interference". In: *Optics & Laser Technology* 141 (2021), p. 107093.
- [33] Zhaokun Wang et al. "Stretched graded-index multimode optical fiber as a saturable absorber for erbium-doped fiber laser mode locking". In: *Optics Letters* 43.9 (2018), pp. 2078–2081.
- [34] Fan Yang et al. "Saturable absorber based on a single mode fiber–graded index fiber–single mode fiber structure with inner micro-cavity". In: *Optics express* 26.2 (2018), pp. 927–934.
- [35] Tao Chen et al. "All-fiber passively mode-locked laser using nonlinear multimode interference of step-index multimode fiber". In: *Photonics Research* 6.11 (2018), pp. 1033–1039.
- [36] Hongwei Zhang et al. "All-fiber nonlinear optical switch based on polarization controller coiled SMF–GIMF–SMF for ultrashort pulse generation". In: *Optics Communications* 452 (2019), pp. 7–11.
- [37] Jikai Chen, DN Wang, and Zhaokun Wang. "Wavelength-switchable multiple type bound solitons in a passively mode-locked Er-doped fiber laser". In: *IEEE Photonics Technology Letters* 32.22 (2020), pp. 1447–1450.
- [38] Guangwei Chen et al. "Generation of coexisting high-energy pulses in a mode-locked all-fiber laser with a nonlinear multimodal interference technique". In: *Photonics Research* 7.2 (2019), pp. 187–192.
- [39] Zhipeng Dong et al. "Er-doped mode-locked fiber lasers based on nonlinear polarization rotation and nonlinear multimode interference". In: *Optics & Laser Technology* 130 (2020), p. 106337.
- [40] Uğur Teğın and Bülend Ortaç. "All-fiber all-normal-dispersion femtosecond laser with a nonlinear multimodal interference-based saturable absorber". In: *Optics letters* 43.7 (2018), pp. 1611–1614.
- [41] Pradeep K Gupta et al. "All-normal dispersion ytterbium-doped fiber laser mode locked by nonlinear multimode interference". In: *Applied Optics* 60.13 (2021), pp. 3888–3894.
- [42] Shuo Chang et al. "Tunable and dual-wavelength mode-locked Yb-doped fiber laser based on graded-index multimode fiber device". In: *Optics & Laser Technology* 140 (2021), p. 107081.

- [43] Shuo Chang et al. “NCF-GIMF device as SA and filter utilized in tunable single-and dual-wavelength Yb-doped mode-locked fiber laser”. In: *Optics Communications* 483 (2021), p. 126612.
- [44] Baofu Zhang et al. “All-fiber mode-locked ytterbium-doped fiber laser with a saturable absorber based on the nonlinear Kerr beam cleanup effect”. In: *Optics Letters* 45.21 (2020), pp. 6050–6053.
- [45] Tao Chen et al. “Evolution of noise-like pulses in mode-locked fiber laser based on straight graded-index multimode fiber structure”. In: *Optics & Laser Technology* 143 (2021), p. 107347.
- [46] Shuo Chang et al. “Generation of coherent multicolor noise-like pulse complex in Yb-doped fiber laser mode-locked by GIMF-SA”. In: *Optics Express* 29.10 (2021), pp. 14336–14344.
- [47] S Thulasi and S Sivabalan. “All-fiber femtosecond mode-locked Yb-laser with few-mode fiber as a saturable absorber”. In: *IEEE Photonics Technology Letters* 33.5 (2021), pp. 223–226.
- [48] Zhipeng Dong et al. “Mode-locked ytterbium-doped fiber laser based on offset-spliced graded index multimode fibers”. In: *Optics & Laser Technology* 119 (2019), p. 105576.
- [49] Zhipeng Dong et al. “Mode-locked fiber laser with offset splicing between two multimode fibers as a saturable absorber”. In: *arXiv preprint arXiv:1807.01037* (2018).
- [50] Wei Pan et al. “All-normal-dispersion dissipative soliton fiber laser using an offset-splicing graded-index-multimode-fiber-based saturable absorber”. In: *Applied Optics* 60.4 (2021), pp. 923–928.
- [51] Zhipeng Dong et al. “Yb-doped all fiber picosecond laser based on grade-index multimode fiber with microcavity”. In: *arXiv preprint arXiv:1809.07174* (2018).
- [52] S Thulasi and S Sivabalan. “Hybrid structure based on no-core and graded-index multimode fibers as saturable absorber for a self-starting mode-locked Yb-doped fiber laser”. In: *Applied Optics* 59.24 (2020), pp. 7357–7363.
- [53] Zhipeng Dong et al. “Generation of mode-locked square-shaped and chair-like pulse based on reverse saturable absorption effect of nonlinear multimode interference”. In: *Optics Express* 27.20 (2019), pp. 27610–27617.
- [54] Zhiguo Lv et al. “Observation of dissipative soliton bound states in a nonlinear multimodal interference based all-fiber all-normal-dispersion mode-locking laser”. In: *Optics & Laser Technology* 119 (2019), p. 105626.
- [55] Zhiguo Lv et al. “Nonlinear multimodal interference for ytterbium-doped all-fiber mode-locking noise-like pulse generation”. In: *Applied Physics Express* 12.2 (2019), p. 022004.
- [56] Huanhuan Li et al. “Mode-locked Tm fiber laser using SMF-SIMF-GIMF-SMF fiber structure as a saturable absorber”. In: *Optics express* 25.22 (2017), pp. 26546–26553.
- [57] Huanhuan Li et al. “Continuously wavelength-tunable mode-locked Tm fiber laser using stretched SMF-GIMF-SMF structure as both saturable absorber and filter”. In: *Optics express* 27.10 (2019), pp. 14437–14446.
- [58] Huanhuan Li et al. “Self-starting mode-locked Tm-doped fiber laser using a hybrid structure of no core-graded index multimode fiber as the saturable absorber”. In: *Optics & Laser Technology* 113 (2019), pp. 317–321.
- [59] Hao Jiang et al. “Mode-locked Tm fiber laser with a tapered GIMF SA based on nonlinear multimode interference effect”. In: *IEEE Photonics Technology Letters* 32.9 (2020), pp. 503–506.
- [60] Huanhuan Li et al. “Generation of switchable multiwavelength solitons with wide wavelength spacing at 2 μm ”. In: *Optics Letters* 44.10 (2019), pp. 2442–2445.
- [61] Arash Mafi et al. “Low-loss coupling between two single-mode optical fibers with different mode-field diameters using a graded-index multimode optical fiber”. In: *Optics letters* 36.18 (2011), pp. 3596–3598.
- [62] Katarzyna Krupa et al. “Multimode nonlinear fiber optics, a spatiotemporal avenue”. In: *APL Photonics* 4.11 (2019), p. 110901.
- [63] Zohar Finkelstein et al. “Spectral shaping in a multimode fiber by all-fiber modulation”. In: *APL Photonics* 8.3 (2023).
- [64] Logan G Wright et al. “Multimode nonlinear fiber optics: massively parallel numerical solver, tutorial, and outlook”. In: *IEEE Journal of Selected Topics in Quantum Electronics* 24.3 (2017), pp. 1–16.
- [65] Ronen Shekel et al. “Tutorial: How to build and control an all-fiber wavefront modulator using mechanical perturbations”. In: *arXiv preprint arXiv:2312.01352* (2023).

Supplementary information

1 Spectral broadening in single-mode fibers

In order to support our claim that the saturable absorption is the result of spectral broadening in the single-mode fiber (SMF), we present the spectral broadening of a pulse propagating in 1m SMF. In Fig. 4 (a) we present the simulated normalized spectrum versus the pulse peak power. At roughly 1kW the pulse spectral width is similar to the spectral scale of change in the multimode fiber (MMF). Therefore, at these powers, we get saturation of the absorption. In figure 4 (b) we present the normalized spectrum versus the pulse peak power, measured by an optical spectrum analyzer (Yokogawa AQ6374).

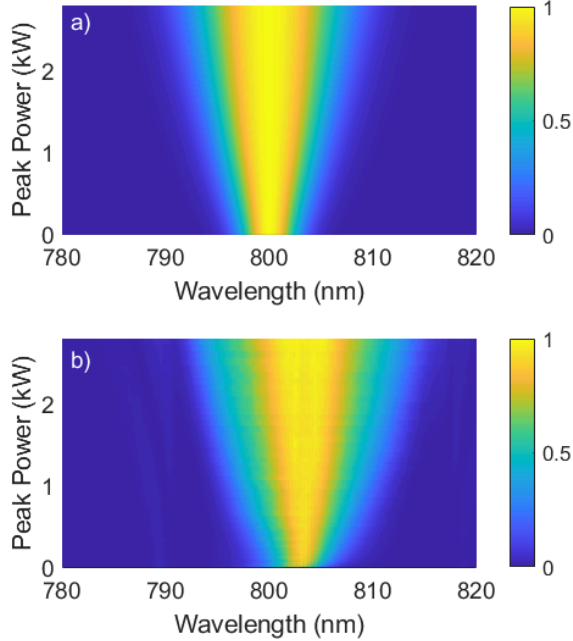


Figure 4: **Spectral broadening in a 1m SMF designed for 780nm** a) Normlized spectrum as a function of the pulse peak power, simulated by a pulse propagation modeled by the nonlinear Schrodinger equation. b) Normalized spectrum as a function of pulse peak measured by an optical spectrum analyzer (Yokogawa AQ6374).

2 Overlap Integrals

To compute the coupling from the SMF to the modes of the MMF, we calculate the overlap integral of the modes:

$$I_k = \left(\frac{\int dxdy F_{SMF}^*(x, y) F_k(x, y)}{\sqrt{\int dxdy |F_{SMF}(x, y)|^2 \int dxdy |F_k(x, y)|^2}} \right)^2 \quad (3)$$

where $F_{SMF}(x, y)$ is the field of the SMF mode and $F_k(x, y)$ is the k th mode of the MMF. In Fig. 5 we present the overlap integrals that have not vanished.

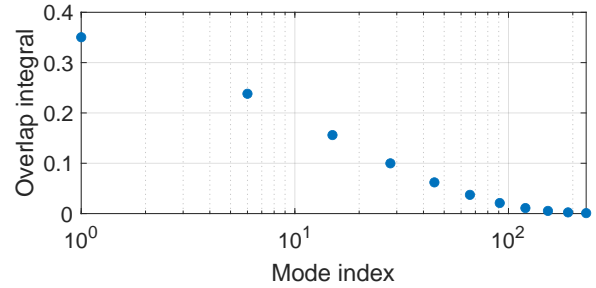


Figure 5: **Computed coupling coefficient between the SMF and MMF modes.** The calculated coupling coefficient between the mode of a $4.4\mu\text{m}$ step index SMF with the modes of a $62.5\mu\text{m}$ graded-index MMF.

3 Bandwidth-induced saturation in multimode fiber-based absorber

Here we calculate transmission as a function of the pulse peak power and central wavelength, using the coupled nonlinear Schrödinger equations (Eq.(1) in the main text). The calculated transmission is presented in Fig. 6(a). To study the contribution of nonlinearity in the MMF, we present in Fig. 6(b) the transmission computed with the linearized version of Eq.(1). In both cases, we initiated a 200fs-wide Gaussian pulse, at the input of the SMF-MMF-SMF device. Here we considered the first two modes of the MMF. Fig. 6 (c) presents the difference between panel (a) and panel (b), showing that the saturated absorption is not induced by intermodal nonlinearity in the MMF, but rather from the MMF bandwidth as explained in the main text.

Last, we calculate the transmission as a function of the peak power of the pulse and its central wavelength, for two multimode fiber lengths Fig. 7. (a,b), showing that the modulation depth is different for different multimode fiber lengths.

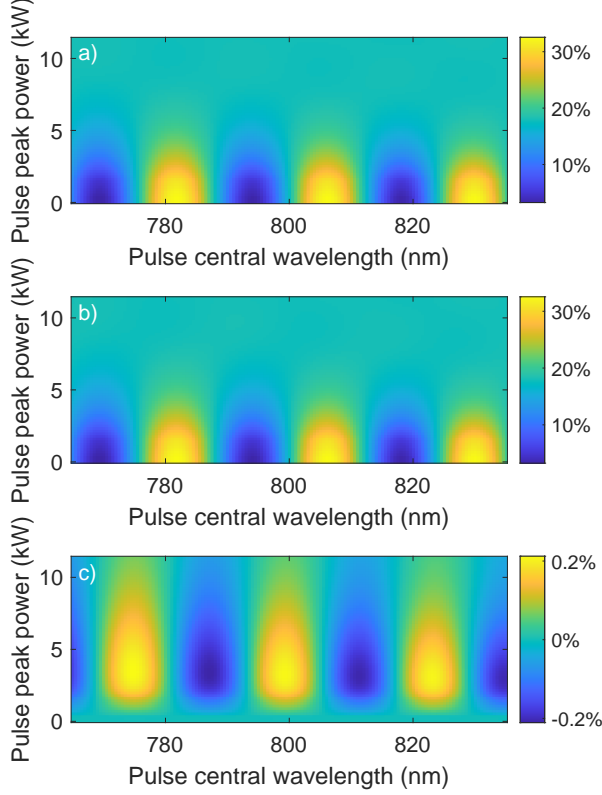


Figure 6: **Wavelength-dependent transmission of a multimode fiber-based saturable absorber.** (a) Transmission calculated according to Eq. 1 (b) and for Eq. 1 without the nonlinear terms in the multimode fiber. The difference between the two cases is presented in (c), showing less than 0.2% difference. Therefore the transmission is not dictated by the intermodal nonlinearities, but rather from the MMF bandwidth as explained in the main text.

4 Intermodal interference and bandwidth-induced saturation in multimode fiber-based absorber

Here we calculate transmission as a function of the pulse peak power and its central wavelength λ_0 using the coupled nonlinear Schrödinger equations (Eq. (1) from the main text), for the low peak power regime (Fig. 8(a)) and the high peak power regime (Fig. 8(b)). In both regimes, we launched a 200fs pulse, at the input of a GRIN MMF. In panel (c) we plot the difference between the transmissions in (a) and (b). In contrast to the results presented in Fig. 3, here the nonlinear terms in the multimode fiber play an important role in the pulse propagation and the saturated absorption.

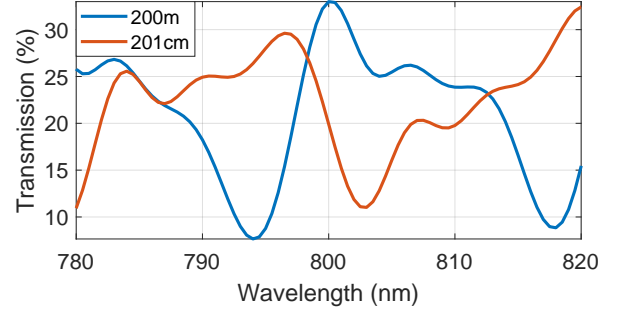


Figure 7: **Linear transmission as a function of the central wavelength of the pulse.** The transmission is calculated for low power pulse and presented as a function of the pulse central wavelength for propagation in s 200cm (a) and 201cm (b) long MMF. The difference between these transmission functions highlights the sensitivity to the fiber length.

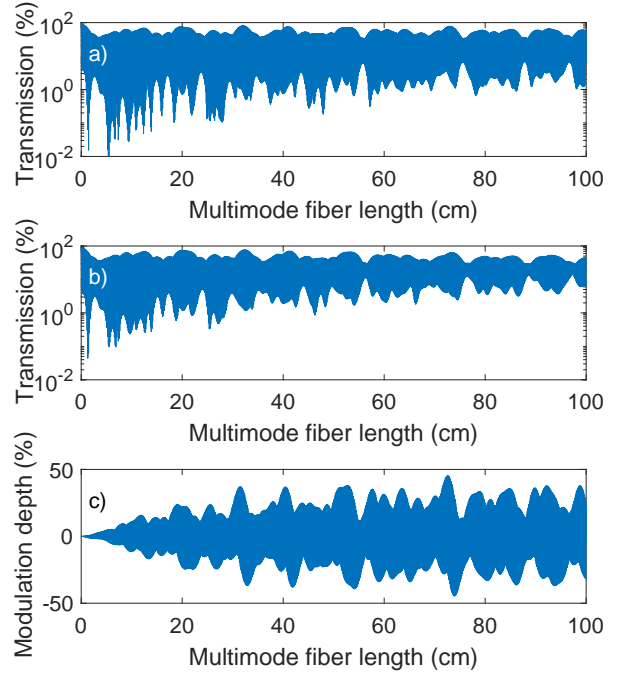


Figure 8: **Nonlinear multimode interference-based saturable absorber.** The calculated coupling transmission for a GRIN multimode fiber to the SMF is presented as a function of the multimode fiber length. The transmission is calculated for low peak powers (a), and high peak powers (b). The modulation depth, calculated by the difference between the transmission for high and low peak powers, is presented in (c). In contrast to the configuration presented in the main text, Fig. 6, here the saturated absorption is induced by both intermodal nonlinearities and the bandwidth mechanism.